ACS OMEGA

Open Access

http://pubs.acs.org/journal/acsodf

Article

Effect of Metal Oxides (CeO_2, ZnO, TiO_2, and Al_2O_3) as the Support for Silver-Supported Catalysts on the Catalytic Oxidation of Diesel Particulate Matter

Punya Promhuad, Boonlue Sawatmongkhon,* Kampanart Theinnoi, Thawatchai Wongchang, Nuwong Chollacoop, Ekarong Sukjit, Sarayut Tunmee, and Athanasios Tsolakis

Cite This: *ACS Omega* 2024, 9, 19282−19294

Read Online

ACCESS | Metrics & More | Article Recommendations

ABSTRACT: This work presented the influence of metal oxides as the support for silver-supported catalysts on the catalytic oxidation of diesel particulate matter (DPM). The supports selected to be used in this work were CeO_2 (reducible), ZnO (semiconductor), TiO_2 (reducible and semiconductor), and Al_2O_3 (acidic). The properties of the synthesized catalysts were investigated using XRD, TEM, H_2-TPR, and XPS techniques. The DPM oxidation activity was performed using the TGA method. Different states of silver (e.g., Ag^0 and Ag^+) were formed with different concentrations and affected the performance of the DPM oxidation. Ag_2O and lattice oxygen, which were mainly generated by Ag/ZnO and Ag/CeO_2, were responsible for combusting the VOCs. The metallic silver (Ag^0) formed primarily on Ag/Al_2O_3 and Ag/TiO_2 was the main component promoting soot combustion. Contact between the catalyst and DPM had a minor effect on VOC oxidation but significantly affected the soot oxidation activity.

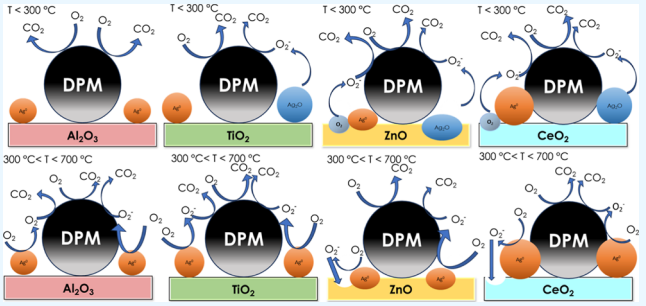

1. INTRODUCTION

In many major cities throughout the world, air pollution has been generally recognized as a serious problem. One of the main causes is typically the burning of fossil fuels. In the transport sector, diesel engines are a significant source of air pollution. These engines release several harmful emissions, including hydrocarbons (HCs), carbon monoxide (CO), nitrogen oxides (NO_x), and particulate matter (PM).[1−3] Especially, PM and NO_x cause major environmental and health issues.[4] Diesel PM (DPM) consists of two main components: a carbon core (called soot) and a volatile organic compound (VOC) coating on the soot.[5] One effective way to reduce DPM emissions is by using a diesel particulate filter (DPF). DPF has two main stages: filtration and regeneration.[6] Filtration involves trapping DPM particles within the porous walls of the DPF, while regeneration uses oxygen to oxidize the entrapped DPM at high temperatures, typically above 600 °C.[5,7−11] Unfortunately, the exhaust gas from a diesel engine is frequently not high enough during normal operation to support the regeneration process.[12,13]

The problem of a low exhaust temperature for DPM oxidation is improved by using oxidation catalyst technology. The oxidation catalyst promotes DPM oxidation by providing a lower energy pathway for the reaction to take place.[14] Oxidation catalysts are often made from noble metals like platinum (Pt), ruthenium (Ru), palladium (Pd), gold (Au), and silver (Ag), which are supported on metal oxide materials including ceria (CeO_2), alumina (Al_2O_3), and silica (SiO_2).[15−20] The addition of an oxidation catalyst can greatly reduce the activation energy required for DPM oxidation, allowing for lower temperatures during DPM combustion. Ag showed special promise among the numerous noble metals examined for use as oxidation catalysts. It was shown that Ag catalysts promoted the generation of adsorbed active oxygen species such as peroxide (O_2^{2-}) and superoxide (O_2^-), which facilitated the oxidation of DPM.[6,18] Ag catalysts exhibited high stability at high temperatures.[21] Moreover, as Ag is less costly than other noble metals, it can be a more cost-effective alternative for use in oxidation catalysts.[6]

The activity of DPM oxidation could be enhanced by using metal catalysts as well as by selecting an appropriate support material. Alumina was widely used as a support of Pt,[22] Cu,[23] and Ag.[15,19,20,24−27] The properties of alumina could influence the activity of catalytic oxidation. Our group[21] investigated the

Received: January 7, 2024
Revised: April 6, 2024
Accepted: April 9, 2024
Published: April 19, 2024

oxidation of DPM using Ag and ceria-supported alumina as the oxidation catalysts. The study showed that Ag coated on alumina at 16 wt % demonstrated excellent DPM oxidation activity and stability. Aneggi et al.[28] studied the behaviors of soot oxidation using Ag deposited on CeO_2, ZrO_2, and Al_2O_3 as the oxidation catalyst. The addition of Ag to ZrO_2 or Al_2O_3 resulted in strong soot oxidation activity under both fresh and aged conditions. Moreover, the acidic support Al_2O_3 plays a crucial role in facilitating the oxidation of soot. In a study conducted by Liu et al.,[29] the investigation focused on the effects of acid sites on the Pt/H-ZSM5 catalyst during the catalytic oxidation of DPM. The research findings indicated that in the presence of surface Pt, the strong acid sites can act as catalysts for the formation and decomposition of surface oxygenated complexes on soot. Consequently, the combined mechanisms of NO_2 and acid-assisted soot oxidation contributed significantly to the exceptional activity observed in the Pt/H-ZSM5 catalyst.

Semiconductor materials have been utilized as catalysts to facilitate and enhance oxidation reactions through their oxygen absorption capabilities. Among these materials, titanium dioxide (TiO_2) stands out as a representative n-type semiconductor that exhibits significant oxygen absorption properties.[30] This characteristic makes TiO_2 particularly suitable for promoting the occurrence of oxidation reactions. Moreover, TiO_2 was identified as another effective oxide support material for PM oxidation. It exhibited strong metal-support interaction (SMSI), high thermal stability, and excellent mechanical strength,[31] which made it a suitable support for various metal catalysts. Additionally, TiO_2 was found to have a high surface area and good dispersion of the metal catalyst, which could further enhance the activity of the catalyst. TiO_2 was utilized in conjunction with Group IB elements, and it was evidenced that larger particle sizes facilitated the occurrence of SMSI compared to smaller particle sizes under high-temperature conditions.[32] Zhang et al.[33] focused on the structure sensitivity between Au and TiO_2 and demonstrated that the presence of SMSI in the Au/TiO_2 catalyst was highly dependent on two factors: the sizes of Au nanoparticles (NPs) and the specific facets of TiO_2. It was also found that Au NPs with an approximate size of 5 nm exhibited a greater tendency to undergo SMSI compared with those with a size of around 2 nm. Furthermore, the (001) and (100) facets of TiO_2 were observed to be more prone to experiencing the SMSI phenomenon than the (101) facet.

Zinc oxide (ZnO) emerges as a compelling semiconductor material that promotes soot oxidation. It exhibited oxygen adsorption capability and a propensity to generate oxygen species on its surface through the formation of oxygen vacancies.[34] Corro et al.[35] conducted a study on the catalytic activity of the Au/ZnO composite in the oxidation of DPM. The authors emphasized the role of bifunctional sites, involving Au° and Au^{3+} species, in enhancing the catalytic performance of the composite. The investigation demonstrated that the 1%Au/ZnO catalyst exhibited both high DPM oxidation activity and remarkable stability. This observation led the authors to conclude that the electronic state of Au and its interactions with the ZnO (n-type semiconductor) played pivotal roles in facilitating the oxidation of DPM. Liu et al.[36] studied the interaction between Au NPs and ZnO nanorods and successfully demonstrated that the SMSI state enhanced CO oxidation.

CeO_2 is one of the most commonly used to support an active metal because of its redox properties and oxygen storage capacity (OSC).[24,37,38] The redox properties (the switching between Ce^{3+} and Ce^{4+}) promoted high OSC performance, resulting in improved soot oxidation performance.[39] An increase in oxygen vacancy can be detected by a decrease in lattice oxygen.[40−42] Setiabudi et al.[43] proposed that CeO_2 facilitated the formation of active oxygen from NO_2 and then stored on CeO_2. However, the desorption and migration of this active oxygen was a slow process compared to the soot oxidation. Alcalde-Santiago et al.[44] used 3DOM ceria catalysts to investigate the contribution of active oxygen and NO_2-assisted soot combustion processes. The results showed that all ceria catalysts accelerated soot combustion with O_2, which occurred mainly through the active-oxygen generation pathway. The mechanisms of soot oxidation using CeO_2 had two main consecutive steps. First, the soot was combusted by lattice oxygen (O_L), which affected the formation of oxygen vacancy (O_v) and reduced CeO_2 (Ce^{4+}) to CeO_{2-x} (Ce^{3+}).[44,45] Then, the gas-phase oxygen adsorbed on the surface of CeO_2 and transformed into active oxygen.[46,47] Lee et al.[39] investigated the effects of Ag quantity on the formation of active oxygen species in Ag-incorporated microporous CeO_2 catalysts for soot oxidation. The authors claimed that the incorporation of Ag as a promoter at a concentration of 5 wt % demonstrated superior combustion efficiency compared to other concentrations. Furthermore, they highlighted the influence of an immoderate Ce^{3+}/Ce^{4+} ratio and the existence of oxygen vacancy in the catalyst, which led to the generation of less reactive oxygen species, specifically O_2^-, as opposed to O^- and O^{2-}.

The active metal and support material properties are critical for promoting DPM oxidation. For example, the morphology and size of the active metal and the oxygen vacancy in the supports played important roles in determining the activity of the oxidation reaction. One property that was found to be particularly significant is the size of the active metal. Small particle sizes have been shown to increase the ionization energy of the catalyst, leading to improved DPM oxidation performance.[48] This was likely due to the increased surface area of the small particles, which allowed for a more efficient interaction with the reactants. The high surface oxygen vacancy of CeO_2 may be favorable for the high performance of the highest CO_2 selectivity,[49] which showed the promotion of oxidation reactions. The OSC of CeO_2 was a critical factor in influencing the soot oxidation activity.[46] The charge state of Ag can be used to distinguish metallic silver (Ag°) from Ag_2O (Ag^+).[14] In general, Ag° has been found to perform better than AgO_x (Ag^+) in promoting soot oxidation.[14,28] Overall, the Ag catalyst and supports' characteristics are critical in determining the DPM oxidation performance. It is possible to create an efficient catalyst for this crucial reaction by carefully regulating these features. However, research on the effect of the support of a Ag catalyst on DPM oxidation has been inconclusive.

This article aims to study the effect of various metal oxides as the support material of Ag catalysts on the performance of DPM oxidation. Ag supported on CeO_2, ZnO, TiO_2, and Al_2O_3 is synthesized and characterized using X-ray diffraction (XRD), high-resolution transmission electron microscopy (HRTEM), hydrogen temperature-programmed reduction (H_2-TPR), and X-ray photoelectron spectroscopy (XPS) techniques. This investigation scrutinizes the influence of catalyst properties, specifically morphology, oxidation state,

https://doi.org/10.1021/acsomega.4c00218
ACS Omega 2024, 9, 19282−19294

and reducibility, on the oxidation activity of DPM. The DPM oxidation activity is assessed by utilizing the thermogravimetric analysis (TGA) method.

2. EXPERIMENTAL SECTION

2.1. Material Preparation. The Ag supported on metal oxides was prepared via incipient wetness impregnation. The silver nitrate (Thomas Baker Chemicals, India) was dissolved in 0.5 cm^3 of distilled water to obtain 16 wt % of Ag on γ-alumina (Ajax Finechem, Australia, BET of 142 m^2/g), titanium oxide (KEMAUS, Australia), ZnO (Quality Reagent Chemical, New Zealand), and 5 wt % of Ag on ceria (Sigma-Aldrich). Then, the precursor solutions were added dropwise to 1 g of the powdered supports. These solvents were dried in an oven at 110 °C overnight and calcined in static air at 600 °C for 2 h. These support materials were chosen because they span a variety of categories, including materials with redox characteristics (CeO_2), transition metal semiconductors (TiO_2), main group semiconductors (ZnO), and acidic materials that are acidic (Al_2O_3). This study selected 16 wt % of Ag because it was the best condition to promote DPM combustion when it was used with Al_2O_3.[21] In the case of Ag/CeO_2, Ag of 5 wt % was selected as it showed the best-promoted soot oxidation.[39]

The diesel engine's exhaust gas served as a direct storage location for the DPM. The engine operated at a speed range of 1000−2000 rpm and a load range of 25−75% of the maximum load. A one-rolled stainless-steel mesh (30 cm length) was inserted in the exhaust pipe (50 mm ID) to trap DPM. Then, the deposited particles were collected and dried in a furnace at 110 °C for 8 h. The dry DPM was kept in an airtight container for upcoming studies.

2.2. Catalyst Characterization. The XRD patterns of the prepared catalysts were identified using a Rigaku Miniflex 600 diffractometer (Rigaku, Japan) with Cu Kα radiation (λ = 1.5418 Å) as an X-ray source. The diffractograms were recorded between 10 and 80° at a scanning rate of 2°/min. Scherrer's equation was used to estimate the average crystallite size.

The textural catalyst images were obtained using HRTEM (Thermo Scientific Talos F200X at 200 kV). The composition of the catalyst was identified by using high-angle annular dark-field scanning transmission electron microscopy (HAADF-STEM) and energy dispersive X-ray spectroscopy (EDS) elemental mapping techniques. Before measurements, the materials were dispersed in ethanol, dropped on 300 mesh carbon-coated grids, and then dried.

The XPS measurement was performed at the end-station of the BL3.2U beamline in the Synchrotron Light Research Institute (SLRI) (Public Organization), Nakhon Ratchasima, Thailand. The beamline photon source had an energy range of 40−1040 eV at a resolving power of 10000. As reported elsewhere, the synchrotron radiation source at the storage ring was generated using a beam energy of 1.2 GeV.[50,51] The XPS was applied to analyze Ag $3d_{3/2}$, Ag $3d_{5/2}$, and O 1s on the top surfaces of the prepared catalysts with excitation photon energy ($h\nu$) at 600 eV. The kinetic energy range of 200−250 eV at a step size of 1.0 eV was used for the wide scan. The Ag $3d_{3/2}$ and Ag $3d_{5/2}$ narrow scans were operated using the same $h\nu$ with a kinetic energy range of 200−250 eV at a step size of 0.1 eV.

The reducibility of catalysts was studied by the H_2-TPR technique using a ChemiSorb 2750 (Micromeritics, United States) equipped with a thermal conductivity detector (TCD). The sample of ∼60 mg was placed in a quartz reactor arranged in a temperature-programmed furnace. Then, the sample was purged with He at 80 °C until the TCD signal was steady (∼30 min). Finally, H_2 (10 vol % in Ar) with a flow rate of 30 mL/min was passed through the sample and heated to 800 °C with a heating rate of 10 °C/min. The TCD signal was recorded continuously to examine the H_2 consumption.

2.3. Catalytic Activity Tests. The catalytic oxidation activity of DPM was examined by using the TGA method (PerkinElmer Pyris 1). The DPM was physically mixed with the catalyst at a weight ratio of 1/5 for 5 min in a stainless-steel mortar to obtain the tight contact mode and was shaken for 5 min in a glass tube for the loose contact condition. Next, the mixture (∼10 mg) was sampled and placed in a ceramic crucible and heated from room temperature to 110 °C with a heating rate of 10 °C/min under N_2, and then the purge gas was switched to O_2 until the temperature reached at 700 °C with a heating rate of 10 °C/min. Purified O_2 (99.99% purity) with a constant flow rate of 50 mL/min was used as the oxidizer. The oxygen concentration (99.99%) was used for the best-case scenario, in which the catalyst could deliver DPM oxidation activity. Furthermore, a high oxygen concentration ensures a sufficient supply of reactant (oxygen) to promote complete oxidation of the DPM sample during the TGA test. This allows for accurate measurement of the DPM's oxidation behavior. The sample weight was recorded continuously with a change in temperature. The DPM oxidation activity was assessed using T_{10}, T_{20}, T_{55}, and T_{90}. T_{10} is the temperature at a 10% weight loss from the initial mass of DPM. It is generally used by the literature to express the beginning of the soot oxidation process.[52] T_{20} represents the temperature at which a weight loss of 20% from the initial mass occurs, indicating the point at which the light VOCs are entirely oxidized. T_{55} identifies the temperature at which all VOCs are completely burned, which is a 55% weight loss from the initial mass.[21] T_{90} corresponds to the temperature at which a 90% weight loss is observed. It is usually employed to indicate the final state of soot oxidation.[53]

3. RESULTS AND DISCUSSION

3.1. XRD. The XRD profiles of Ag/CeO_2, Ag/ZnO, Ag/TiO_2, and Ag/Al_2O_3 are demonstrated in Figure 1. The peaks

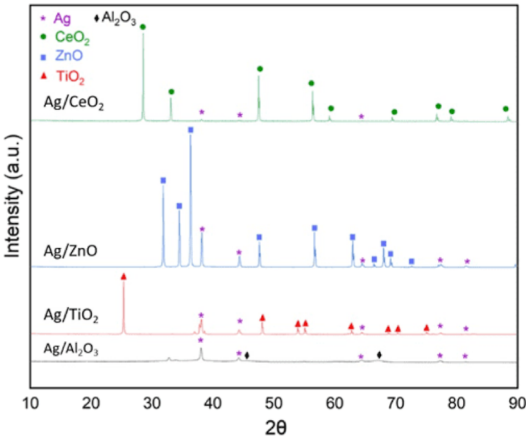

Figure 1. XRD profiles of Ag/CeO_2, Ag/ZnO, Ag/TiO_2, and Ag/Al_2O_3.

https://doi.org/10.1021/acsomega.4c00218
ACS Omega 2024, 9, 19282−19294

of metallic silver (Ag°) are indicated by the JCPDS 04-0783 database.[54−58] Two diffraction peaks of Ag° at 38 and 44° were commonly reported in the literature.[24,55,56] Ag_2O is not detected on all catalysts. The detection of Ag_2O by XRD depends on the support used. Corro et al.[59] found a signal of Ag_2O at 32° on both Ag/SiO_2 and Ag/ZnO. In contrast, Shimizu et al.[47] and Aneggi et al.[28] did not observe Ag_2O on Ag/CeO_2, Ag/ZrO_2, and Ag/Al_2O_3. Aneggi et al.[28] suggested that in Ag/CeO_2 and Ag/ZrO_2, Ag_2O was formed first and then rapidly transformed into metallic Ag during calcination. The remaining Ag_2O obtained a low concentration and a small size (5 nm), which were beyond the detection ability of XRD.[21,28] The peaks of TiO_2 indicate the anatase type of TiO_2, which is the most stable crystal of TiO_2 polymorphs (e.g., anatase, brookite, and rutile).[60] The peaks of Al_2O_3 refer to the gramma type of alumina (γ-Al_2O_3).[61] Ag/CeO_2 shows the low intensity of the Ag peak compared to other catalysts because the percentage of Ag in CeO_2 is 5 wt %, while others are 16 wt %.

Table 1 presents the interplanar distance (d_{hkl}) and the average crystallite size of Ag°, which were calculated using

Table 1. Interplanar Distance (d_{hkl}) at (111) and (200) and the Average Crystallite Size of Ag°

sample	miller indices at (111) of Ag°		miller indices at (200) of Ag°		average crystallite size (nm) of Ag°
	2θ	d_{111} (Å)	2θ	d_{200} (Å)	
Ag/CeO_2	38.10	2.36	44.30	2.04	40.73
Ag/ZnO	38.16	2.36	44.36	2.04	14.99
Ag/TiO_2	38.12	2.36	44.32	2.04	13.37
Ag/Al_2O_3	38.06	2.36	44.26	2.05	10.68

Bragg's law and Scherrer's equation. The lattice constants of (111) and (200) are 2.36 and 2.04 Å, respectively, indicating the Ag° on support.[24] The average crystallite sizes of Ag° on supports increase in the following order: Ag/Al_2O_3 (10.68 nm), Ag/TiO_2 (13.37 nm), Ag/ZnO (14.99 nm), and Ag/CeO_2 (40.73 nm). The difference in crystallite size explains why different supports affect the active metal dispersion and metal-support interaction (MSI) differently.

3.2. HRTEM. Figure 2 shows the structure of the Ag catalysts on different supports presented in the HRTEM images. The interplanar distance of the crystal planes in the case of Ag/CeO_2 is 0.204 nm, which indicates the Ag° at Miller indices of (200). This is consistent with the result obtained from XRD at 2θ = 44.3°. The interplanar distance of Ag_2O is found by HRTEM only in the case of Ag/ZnO at 0.27 nm, which illustrates Miller indices of (111).[24] In the case of Ag/TiO_2, d_{111} of 0.236 nm matches with Ag° at XRD of 2θ = 38.16°. The Miller indices of Ag° at (111) and (200) are discovered in Ag/Al_2O_3, which are d_{111} = 0.236 nm and d_{200} = 0.205 nm. The HRTEM was suggested by Liu[62] to indicate the type of MSI. All catalysts in this work except Ag/ZnO present weak MSIs (WMSIs) because this study uses the incipient wetness impregnation method for catalyst preparation. The WMSI is consistent with the results presented by Grabchenko et al.[24] In the case of Ag/ZnO, it exhibits SMSI due to the tendency of ZnO to be SMSI when it is synthesized with Au, Ag, Pd, and Pt.[63] In general, the SMSI induces metal NP encapsulation, which, accordingly, reduces the catalytic activity

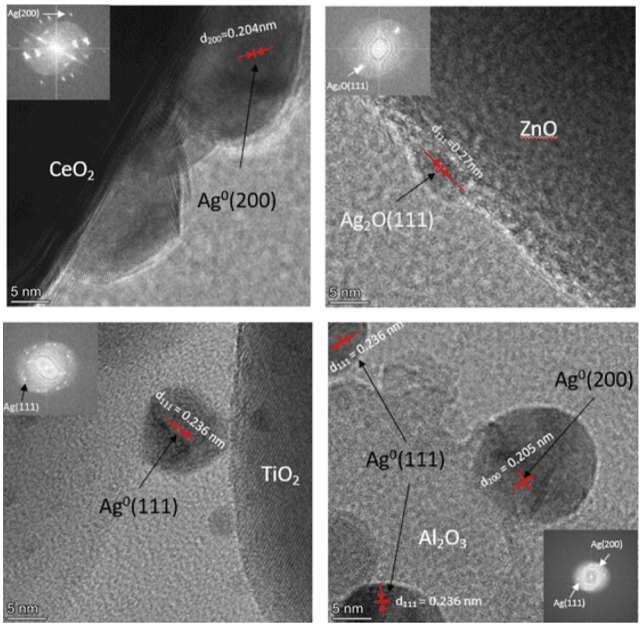

Figure 2. HRTEM images of Ag/CeO_2, Ag/ZnO, Ag/TiO_2, and Ag/Al_2O_3.

of supported metal catalysts due to the blockage of active metal sites.[64,65]

Figure 3 displays the HAADF-STEM images and mapping of Ag on oxide supports. The images present the compositions of Ag/CeO_2, Ag/ZnO, Ag/TiO_2, and Ag/Al_2O_3, which are identical to the components found in the XRD. The STEM mapping confirms that small particles and clusters of Ag are impregnated adjacent to the oxide supports. The distribution of Ag on Al_2O_3 can be observed, showing that the Ag particles are small and evenly dispersed across the entire surface area of the support. However, in the case of Ag/TiO_2, clusters of Ag begin to form, and their dispersion becomes less pronounced. Dense clusters of Ag appear on the support in the cases of Ag/ZnO and Ag/CeO_2. The difference in the distribution of Ag NPs impacts the performance of DPM oxidation. This is because of the interaction between the catalyst and DPM, which is influenced by the catalyst particle size.[66] Smaller catalyst particles provide a larger surface area, which promotes closer and more effective contact.[21,67]

3.3. XPS. The XPS method was frequently used to characterize and determine the electronic states of catalysts.[39,68] Figure 4 presents the binding energy of the fresh catalyst, which is the Ag catalyst on the oxide support. The estimation of the peak of Ag intensities involves the assessment of each peak's integral after subtracting a background characterized by an S-shaped curve. Additionally, Gaussian curves are fitted to the experimental peak data to model the observed distribution. The peak deconvolution indicates the presence of both Ag° and Ag^+. The binding energies of Ag° are 368.4 (Ag $3d_{5/2}$) and 374.5 (Ag $3d_{3/2}$) eV, while those of Ag^+ are 367.8 (Ag $3d_{5/2}$) and 373.9 (Ag $3d_{3/2}$) eV.[66] The magnitude of both binding energies can be used to determine the extent of each oxidation state.[39,68] According to Liu et al.,[69] an estimation of oxygen species concentrations was achieved by calculating the ratio of $[O_v]$ (oxygen vacancy) to $([O_v]+[O_l])$ (combined oxygen vacancy and lattice oxygen). The authors utilized the peak area of each oxygen species to determine the $[O_v]/([O_v]+[O_l])$ ratio. This work applies the

https://doi.org/10.1021/acsomega.4c00218
ACS Omega 2024, 9, 19282−19294

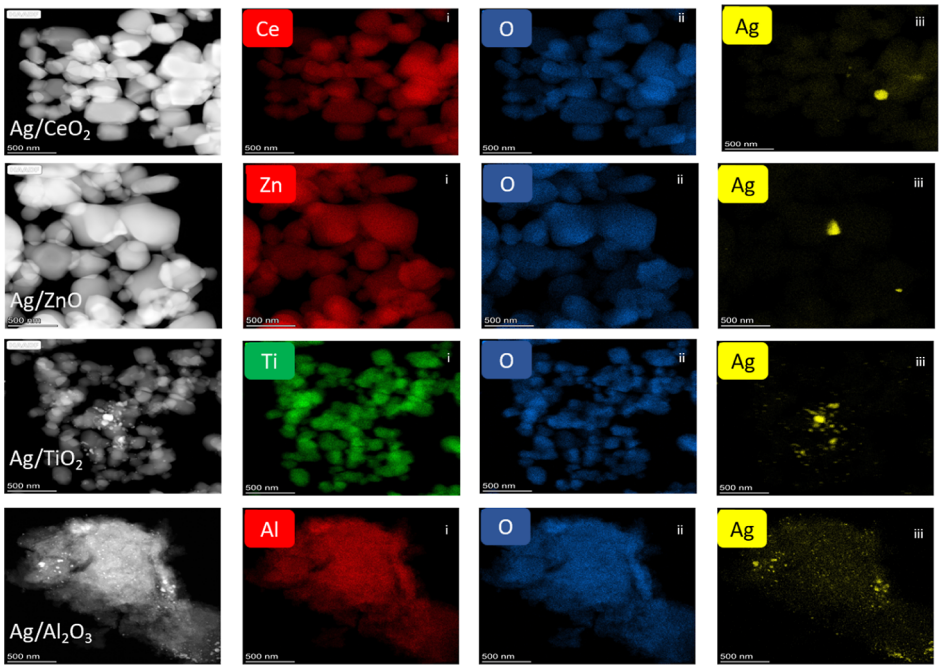

Figure 3. HAADF-STEM and EDS elemental mapping images of Ag/CeO_2, Ag/ZnO, Ag/TiO_2, and Ag/Al_2O_3.

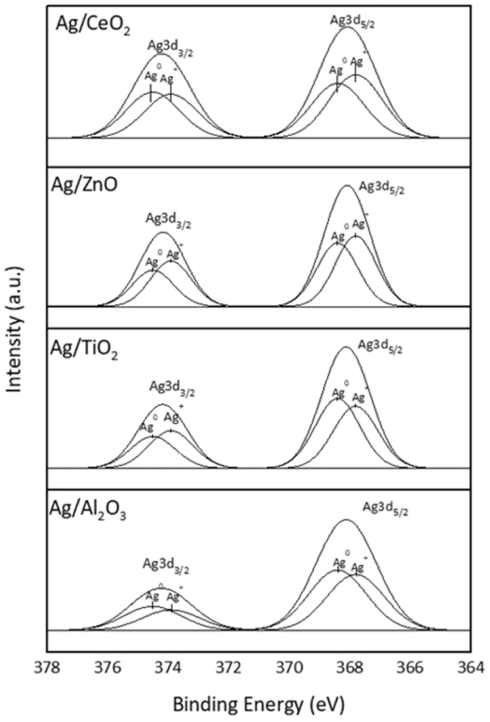

Figure 4. XPS spectra of the fresh catalysts of Ag $3d_{3/2}$ and Ag $3d_{5/2}$ of Ag/CeO_2, Ag/ZnO, Ag/TiO_2, and Ag/Al_2O_3.

same technique to determine the quantities of Ag° and Ag^{+}. The areas of Ag° and Ag^{+}, the percentage of Ag° and Ag^{+}, and the Ag°/Ag^{+} ratio are calculated and presented in Table 2. The percentage of Ag° follows the order Ag/Al_2O_3, Ag/TiO_2, Ag/ZnO, and Ag/CeO_2, but the reverse is observed for the percentage of Ag^{+}, with Ag/CeO_2 being the highest. These variations in the percentages of Ag° and Ag^{+} are attributed to the choice of different support materials, resulting in consequential effects on the type and quantity of active oxygen

Table 2. Percentage of the Oxidation State of Ag (Ag° and Ag^{+}) and Ag°/Ag^{+} Ratio

catalyst	area of Ag°	area of Ag^{+}	Ag°	Ag^{+}	Ag°/Ag^{+}
Ag/CeO_2	3.7	4.7	43.9	56.06	0.78
Ag/ZnO	13.2	15.3	46.3	53.71	0.86
Ag/TiO_2	16.1	15.8	50.5	49.47	1.02
Ag/Al_2O_3	24.4	22.0	52.6	47.40	1.11

formed, thus influencing the oxidation performance of the DPM.

The determination of binding energies in the O 1s XPS spectra reveals distinct peaks at 529.4, 530.4, and 532.3 eV.[24,39] This characterization of oxygen species, encompassing oxygen vacancy (O_v), lattice oxygen (O_l), and adsorbed oxygen (O_c), assumes pivotal significance in elucidating the oxidation-promoting attributes of DPM, as illustrated in Figure 5. Analysis reveals that in the systems Ag/TiO_2 and Ag/Al_2O_3, only O_l and O_c are present, as confirmed by the results of H_2-TPR, which display two distinct peaks corresponding to oxygen species. Specifically, in the case of Ag/TiO_2, the composition of O_l and O_c accounts for 94.93 and 5.7% of all oxygen species, respectively. Ag/Al_2O_3 shows O_c (12.47%) and O_l (87.53%). In the instances of Ag/ZnO and Ag/CeO_2, the presence of O_l, O_v, and O_c was confirmed through H_2-TPR, which exhibited two peaks indicative of hydrogen consumption. Specifically, in the case of Ag/CeO_2, the composition of O_c, O_v, and O_l accounted for 18.32, 39.56, and 42.11%, respectively. Conversely, in the case of Ag/ZnO, the percentages were 39, 46.98, and 14.02%, respectively. These findings underscore the significance of different oxide supports and their interactions with varying types and concentrations of oxygen species, thereby contributing to the oxidation-promoting behaviors observed.

The interactions between the metal catalyst and the support materials are pivotal in shaping their catalytic properties. These interactions are multifaceted, encompassing chemical, electronic, and structural. First, the varying chemical affinities of

https://doi.org/10.1021/acsomega.4c00218
ACS Omega 2024, 9, 19282−19294

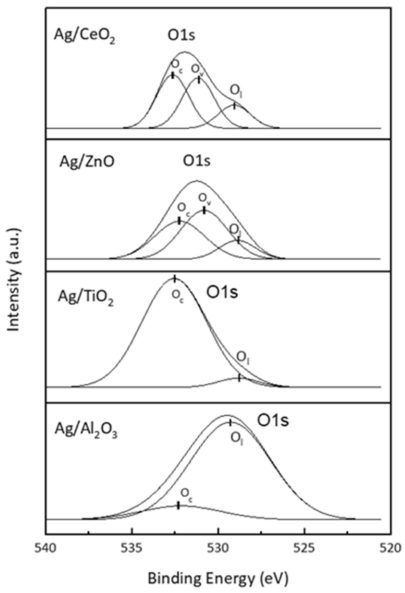

Figure 5. XPS spectra of fresh catalysts of O 1s of Ag/CeO_2, Ag/ZnO, Ag/TiO_2, and Ag/Al_2O_3.

different support materials toward metal species influence their adsorption, dispersion, and stabilization on the support surface. Additionally, the electronic properties of oxide supports play a crucial role in modulating the oxidation states of the metal species. For example, redox-active supports like ceria (CeO_2) can facilitate electron transfer reactions, thereby influencing the distribution of metal species and their catalytic activity. Moreover, surface chemistry parameters such as defects, surface functional groups, and crystallographic planes dictate the adsorption and activation of reactant molecules, which are pivotal for catalytic oxidation reactions. Furthermore, oxide supports can stabilize active sites, such as oxygen vacancies, which are crucial for catalytic activity.

3.4. H_2-TPR. The H_2-TPR technique is employed to analyze the reducibility characteristics of the catalysts, as depicted in Figure 6. The release of oxygen from the catalyst is identified through the H_2-TPR profile. Ag_2O is reduced as follows:[70] $Ag_2O + H_2 \rightarrow 2Ag^\circ + H_2O$. The atomic oxygen separated from Ag_2O was defined as active oxygen, and it formed at temperatures below 300 °C. As a result, at a temperature higher than 300 °C, Ag_2O completely changed to Ag°.[66]

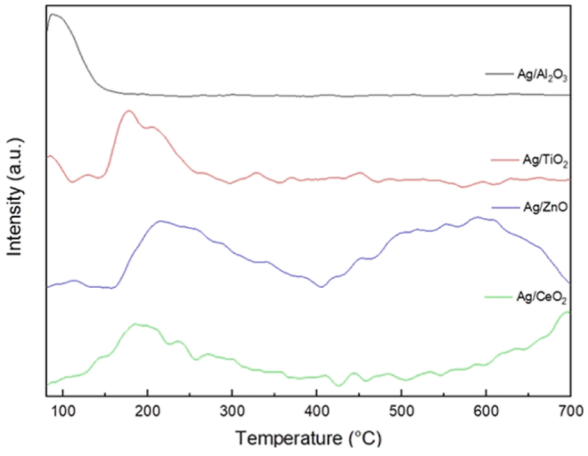

Figure 6. H_2-TPR profiles of Ag/Al_2O_3, Ag/TiO_2, Ag/ZnO, and Ag/CeO_2.

Ag/Al_2O_3 shows one peak of the H_2-TPR profile at around 100 °C. This peak is at a temperature lower than 300 °C, which identifies the reduction of Ag_2O since Al_2O_3 is not reduced at this temperature range.[67,71] Ousji et al.[67] studied Ag-based catalysts on different supports for formaldehyde oxidation and used the H_2-TPR to determine the reducibility of metal oxides. In the case of Ag/Al_2O_3, the authors found a reduction of peak Ag_2O at around 100 °C. Additionally, the absence of the TCD peak indicates that there is no catalyst-driven oxygen release at temperatures exceeding 150 °C. Our result is also in line with Aneggi et al.,[28] who found that there were no H_2-TPR traces of both Ag/Al_2O_3 and Ag/ZrO_2 at temperatures higher than 110 °C. Based on these experimental findings, it can be confirmed that Ag_2O in Ag/Al_2O_3 is readily and fully converted to Ag° once it is reduced by H_2.

Ag/TiO_2 indicates one peak of H_2-TPR at 150−250 °C. Boccuzzi et al.[72] studied Au, Ag, and Cu catalysts supported by TiO_2 for hydrogen production. The H_2-TPR peak of Ag/TiO_2 was found at 150 °C. Moreover, Kim et al.[14] used ceria to promote Ag/TiO_2 for soot oxidation with improved active oxygen generation and delivery abilities. The authors presented the H_2-TPR peak of Ag/anatase between 250 and 330 °C. These H_2-TPR results are like the reducibility characteristics of Ag/TiO_2 presented in this study. The H_2 consumption at 150−250 °C is likely attributed to the reduction of Ag_2O, as significant amounts of Ag_2O are also detected by XPS.

Ag/ZnO shows two peaks of H_2-TPR at around 200 and 600 °C, which express the reduction of Ag_2O and lattice oxygen in the ZnO bulk, respectively. The transformation of Zn^+ to Zn° follows $ZnO + H_2 \rightarrow Zn^\circ + H_2O$. This conversion was also identified on Cu/ZnO.[73] Zhao et al.[74] studied the CeO_2−ZnO catalysts for C_3H_6-SCR of NO and found that the H_2-TPR peak of ZnO appeared obviously at 600 °C. Accordingly, the H_2-TPR peak at 600 °C in this work is presumably the release of oxygen from the lattice of ZnO.

Ag/CeO_2 obtains two peaks of H_2 consumption at around 200 and 700 °C, corresponding to the reduction of Ag_2O and lattice oxygen in Ag/CeO_2. In the H_2-TPR of CeO_2, Queiroz et al.[75] showed two reduction peaks: one at 456 °C attributed to the reduction of CeO_2 species on the surface, and another one at 790 °C stood for that of CeO_2 containing bulk. Wei et al.[76] and Yao et al.[77] pointed out the peaks at low (400 °C) and high (500 °C) temperatures to the reduction of surface adsorbed oxygen and lattice oxygen of ceria, respectively. The presence of Ag was found to facilitate the reduction of surface oxygen of CeO_2.[39,78] Lee et al.[39] suggested that the reduction peak at 167−222 °C of Ag/CeO_2 represented not only the reduction of Ag_xO but also the reduction of surface oxygen of ceria. Furthermore, Grabchenko et al.[24] studied the role of MSI in Ag/CeO_2 catalysts for CO and soot oxidation, and the authors showed H_2 consumption in the temperature range of 0−350 °C. Therefore, it can be implied that the first peak at around 200 °C in this study characterizes the reduction of both Ag_2O and surface oxygen of CeO_2.

The support has an impact on the reducibility of the catalysts, as indicated by the variation in the peak temperature of the H_2-TPR profile. This variation describes the differences in the reduction behaviors of active oxygen generated from Ag in the form of Ag_2O, from the surface of support (e.g., Ag/CeO_2), and from the lattice of support (e.g., Ag/ZnO and Ag/CeO_2). Consequently, the utilization of the created active

https://doi.org/10.1021/acsomega.4c00218
ACS Omega 2024, 9, 19282−19294

oxygen for the oxidation of DPM leads to alterations in its activity, thus highlighting the influence of support selection on the catalytic performance.

3.5. Catalytic Oxidation of DPM. Figure 7 illustrates the catalytic oxidation activity of DPM accelerated by the synthesized catalysts. The percentages of weight loss and the first derivative of weight loss (DTG) are shown in Figure 7a,b, respectively. Without any catalyst, the DPM is oxidized slowly and monotonously, starting from 200 °C, until it is entirely converted at 650 °C. The DTG of DPM in the absence of a catalyst, Figure 6b, shows three peaks at 230, 380, and 500 °C. The first two peaks at relatively low temperatures indicate the combustion of VOCs. Light VOCs consisting mainly of straight-chain HCs are burned first at low temperatures. Then, polycyclic aromatic hydrocarbons and heavy VOCs are combusted at high temperatures.[21] Finally, solid carbon (soot) is oxidized at temperatures of 400−650 °C.[20,21,79] This implies that amorphous and nanofiber carbons, which are noncatalytically oxidized with oxygen at 200−500 °C and 500−600 °C, respectively,[80,81] are the main components of diesel soot. Graphitic carbon, which is combusted at 600−800 °C, is not found in the PM of diesel-engine exhaust.

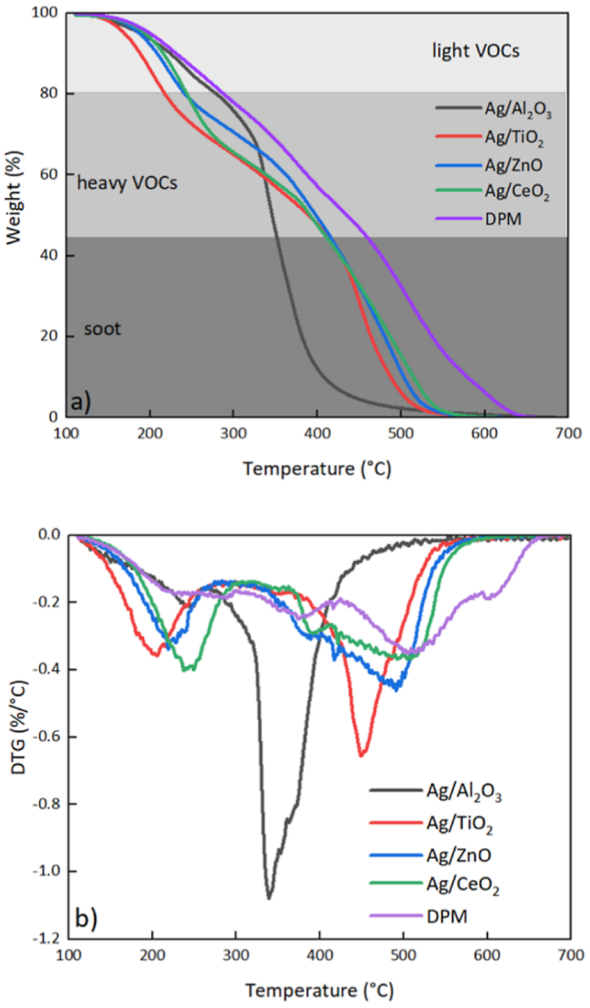

Figure 7. (a) DPM oxidation and (b) first derivative of DPM oxidation; DPM/catalyst weight ratio of 1/5; heating rate of 10 °C/min; and tight contact.

In the presence of Ag/Al_2O_3, the light VOCs are converted in the same manner as the noncatalytic path, which informs that the oxidation of light VOCs is not improved by Ag/Al_2O_3. In contrast, the oxidation of heavy VOCs and soot is strongly promoted by Ag/Al_2O_3. The temperature corresponding to the complete conversion of heavy VOCs is reduced from 459 to 352 °C, and all soot is completely removed at the temperature of 540 °C instead of 650 °C in the absence of a catalyst. The high fraction of Ag° as evidenced by HRTEM and XPS is responsible for this promotion.

In the case of Ag/TiO_2, the combustion of the VOCs is substantially improved. Both light and heavy VOCs are oxidized simultaneously as their DTG peaks are combined and shown as a single peak at 205 °C. This is the lowest temperature among other catalysts, suggesting that Ag/TiO_2 is suitable for VOC removal. The active oxygen generated in the form of Ag_2O on the surface of Ag/TiO_2 as shown in H_2-TPR is behind this promotion effect. All DPM is completely burned off at around 550 °C, which is the same temperature as that for Ag/Al_2O_3. However, the combustion rate of Ag/TiO_2 is much lower than that of Ag/Al_2O_3. For example, at 430 °C, 95% of DPM is combusted by Ag/Al_2O_3, while only 60% is converted by Ag/TiO_2. Moreover, the T_{90} values of both catalysts are markedly different. The T_{90} values of Ag/Al_2O_3 and Ag/TiO_2 are 408 and 488 °C, respectively.

The DPM oxidation characteristic catalyzed by Ag/ZnO differs from that of Ag/Al_2O_3 and Ag/TiO_2. The DTG profile indicates a peak at 220 °C, a shoulder at 390 °C, and a peak at 492 °C, which correspond to the maximum oxidation rates of light and heavy VOCs, and soot, respectively. As the Ag_2O formed on Ag/ZnO is reduced at 150−400 °C (from the H_2-TPR result), this reveals that active oxygen released from Ag_2O is responsible for the combustion of light and heavy VOCs. The oxidation of carbonaceous solids, then, takes place after the oxidation of VOCs at a temperature of 450−550 °C. The lattice oxygen, which is released from ZnO at 400−700 °C, as given in H_2-TPR, is one of the oxidizers.[73] Moreover, the metallic silver generated previously from the reduction of Ag_2O by VOCs acts as an active site on which gas-phase oxygen to adsorb on. In summary, the oxidation of soot on Ag/ZnO is facilitated either by lattice or gas-phase oxygen.

Ag/CeO_2 gives DPM oxidation activity like Ag/ZnO. The DTG profile shows three peaks at 245, 389, and 508 °C, which are attributed to the maximum oxidation rates of light and heavy VOCs and soot, respectively. As presented in the H_2-TPR, the active oxygen is removed from the Ag/CeO_2 surface at temperatures lower than 200 °C, but the combustion of VOCs takes place at temperatures higher than 200 °C. This implies that the active oxygen migrates from the catalyst surface to DPM first, and the catalytic burnout of VOCs initiates later. The high fraction of Ag^+ of Ag/CeO_2 (shown in Table 2) illustrates the fast rate of VOC decomposition. The oxidation rate of solid carbon is relatively low and occurs at relatively high temperatures compared with other catalysts. The small amount of Ag° on the surface of Ag/CeO_2 (Table 2) results in less soot oxidation than in other cases. The metallic silver could promote the formation of active oxygen species (O_2^-) that was the main oxidizer to assist the soot oxidation.[28,82] Corro et al.[59] studied the electronic state of Ag in Ag/SiO_2 and Ag/ZnO catalysts. The authors concluded that the presence of Ag° on the surface of the composite catalysts produced a large amount of O_2^-, which was a particularly active species for enhancing DPM oxidation. This

https://doi.org/10.1021/acsomega.4c00218
ACS Omega 2024, 9, 19282−19294

can be summarized as Ag^+ (which is derived from Ag_2O) contributing to the combustion of VOCs, while Ag° facilitates the adsorption of gas-phase oxygen to generate active oxygen needed to oxidize with soot.

The temperature range at which Ag_2O is reduced significantly impacts the combustion of light VOCs. In the case of Ag/Al_2O_3, the release of active oxygen from Ag_2O occurs at a temperature range of 80−150 °C (Figure 6), which is lower than the starting point of light VOC combustion (Figure 7). Consequently, no active oxygen remains to initiate the oxidation of light VOCs. In contrast, in the case of Ag/TiO_2, the catalyst gives the best performance of light VOC combustion. This can be attributed to the temperature-dependent release of active oxygen from Ag_2O, which is suitable for triggering the combustion of light VOCs within the appropriate temperature range. Interestingly, although Ag_2O on Ag/TiO_2 and Ag/CeO_2 have a similar reduction temperature (Figure 6), Ag/TiO_2 produces a higher quantity of Ag_2O (a higher area of Ag^+ in Table 2). These experimental findings reveal that not only the temperature range in which atomic oxygen is released from Ag_2O but also the amount of active oxygen is responsible for burning off light VOCs. The choice of support material influences these factors and, thereby, affects the characteristics of light VOC combustion.

Figure 8 demonstrates the performance of synthesized catalysts for DPM oxidation. T_{10} increases in the following order: Ag/TiO_2 (189 °C), Ag/ZnO (209 °C), Ag/CeO_2 (217 °C), Ag/Al_2O_3 (225 °C), and DPM (232 °C). The peak temperatures of H_2-TPR (Figure 6) and T_{10} of Ag/TiO_2, Ag/ZnO, and Ag/CeO_2 are strongly related. It implies that the active oxygen generated by these catalysts is crucial for initiating the combustion of light VOCs. Despite having the lowest peak temperature in H_2-TPR (approximately 100 °C), Ag/Al_2O_3 appears to be less effective than other catalysts in initiating the oxidation of light VOCs. Also, it was stated that VOCs inherent in DPM made lower ignition temperature and faster combustion rate than carbon black (which was usually used in the literature as model DPM).[52,83]

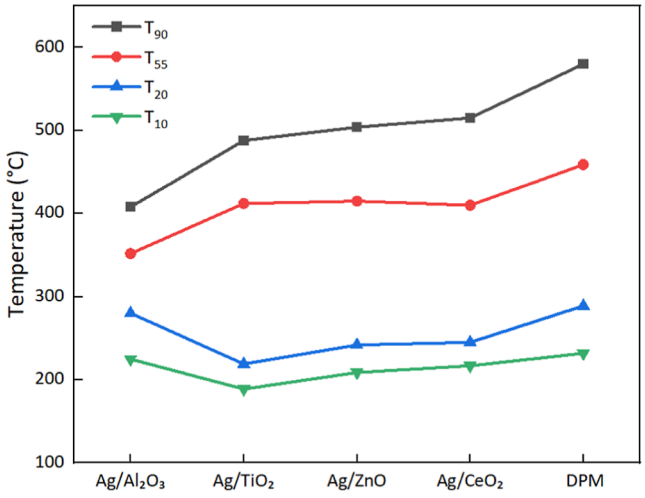

Figure 8. DPM oxidation performance of Ag with different supports; DPM/catalyst weight ratio of 1/5; and tight contact.

T_{20} states the capability of catalysts for entirely oxidizing light VOCs. Figure 8 clearly shows that T_{20} is in the same trend as T_{10}. Ag/TiO_2, Ag/ZnO, and Ag/CeO_2 show high performance, while Ag/Al_2O_3 gives the lowest activity (highest T_{20}). The weak bonding between atomic oxygen and Ag leads to the reduction of Ag_2O into fundamental metallic silver at exceptionally low temperatures, as previously discussed, resulting in the low activity of Ag/Al_2O_3. This observation is substantiated by the outcomes of the H_2-TPR analysis conducted at temperatures below 100 °C. The discerned occurrence can be attributed to the Al_2O_3-type support material facilitating the interaction between oxygen and Ag. This phenomenon permits the desorption of oxygen from Ag_2O at lower temperatures compared to those of other scenarios. Moreover, the manifestation of oxygen release at reduced temperatures aligns with findings reported by Aneggi et al.,[28] where the influence of H_2-TPR was not evident in the case of Ag/Al_2O_3 at elevated temperatures. It can be posited that Al_2O_3 exerts an influence on the interaction between oxygen and the Ag bond, resulting in a diminished bond strength and consequently facilitating oxygen desorption at lower temperatures. Consequently, the oxygen needed to oxidize light VOCs must be sourced directly from the gas-phase oxygen. The evidence is given in Figure 7 that the light VOC oxidation activities of Ag/Al_2O_3 and DPM (without catalyst) are identical.

T_{55} indicates the point at which both light and heavy VOCs are entirely burned off. The potential for depleting VOCs is in the following order: Ag/Al_2O_3 (352 °C) > Ag/CeO_2 (410 °C) ~ Ag/TiO_2 (412 °C) ~ Ag/ZnO (415 °C) > PM (459 °C). Surprisingly, although Ag/Al_2O_3 has the lowest performance of light VOC oxidation, it is the best catalyst for the combustion of all VOCs. This reveals that the active oxygen produced by Ag/Al_2O_3 is more active with heavy VOCs than that yielded by Ag/TiO_2, Ag/ZnO, and Ag/CeO_2. According to Table 2, Ag/Al_2O_3 has the highest values of Ag° area, Ag° fraction, and Ag°/Ag^+ ratio, and the H_2-TPR result demonstrates that at temperatures above 150 °C, there is no oxygen released from Ag/Al_2O_3. It can be concluded that the active oxygen generated by Ag/Al_2O_3 is directly formulated from gas-phase oxygen, mainly on the Ag° sites.

Ag/Al_2O_3 gives the lowest value of T_{90}, which highlights the positive effect of Ag/Al_2O_3 on solid-carbon combustion. Ag° is the major species generated on the Ag/Al_2O_3 surface, and it functions as the active site necessary for the adsorption of gas-phase oxygen to produce highly active oxygen. This active oxygen is particularly reactive with both heavy VOCs and soot. The performance of soot oxidation as expressed by T_{90} is in the order of Ag/Al_2O_3 (408 °C), Ag/TiO_2 (488 °C), Ag/ZnO (504 °C), Ag/CeO_2 (515 °C), and DPM (580 °C), which relates directly to the amount of Ag° created by the catalysts (Table 2).

Figure 9 illustrates the sensitivity of DPM catalytic oxidation to the contact condition. In the case of Ag/Al_2O_3, as depicted in Figure 9a, since Ag_2O formed on Ag/Al_2O_3 is easily reduced at low temperatures (shown in H_2-TPR), there is no active oxygen from Ag_2O remaining for the oxidation of light VOCs. A slight improvement in the oxidation of light and heavy VOCs for the loose contact expresses that the active oxygen is directly formulated from gas-phase oxygen on Ag° sites. The higher activity of loose contact than tight contact is probably due to its low site blockage (higher catalyst surface exposed to gas-phase oxygen). For the oxidation of soot, loose contact exhibits a much lower performance compared to tight contact. This suggests that the active oxygen created by Ag° of Ag/

https://doi.org/10.1021/acsomega.4c00218
ACS Omega 2024, 9, 19282−19294

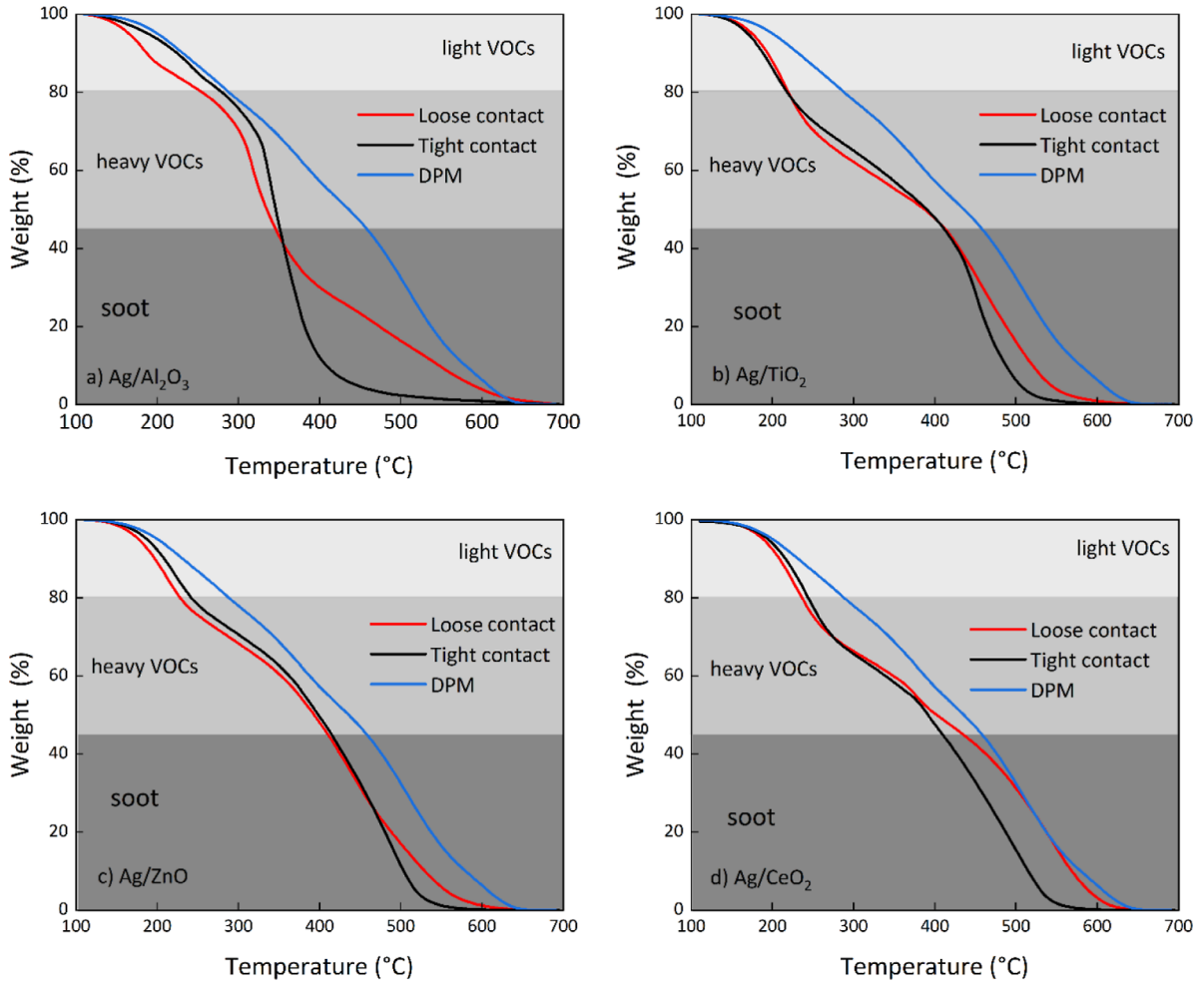

Figure 9. Influence of contact condition on the catalytic oxidation of DPM catalyzed by (a) Ag/Al_2O_3, (b) Ag/TiO_2, (c) Ag/ZnO, and (d) Ag/CeO_2; DPM/catalyst weight ratio of 1/5; and heating rate of 10 °C/min.

Al_2O_3 has a low ability to migrate from the catalyst sites to soot.

Figure 9b shows that for the catalytic combustion of light and heavy VOCs promoted by Ag/TiO_2, the oxidation profiles of tight and loose contacts are identical. As previously mentioned, Ag_2O is responsible for the light VOC oxidation under tight contact conditions. The equivalent activity for light VOC depletion of tight and loose contacts suggests that active oxygen created from Ag_2O has a high degree of mobility. In contrast, the active oxygen formulated on Ag° sites contributes to the combustion of heavy VOCs and soot. The similar pattern for heavy VOCs elimination of the tight and loose contacts states that the active oxygen on Ag° can readily transfer to a hydrogen atom of VOCs. Nonetheless, this active oxygen has a low ability to migrate from the Ag° sites to a carbon atom of soot, which is indicated by the discrepancy in combustion performance of the loose and tight contacts.

For Ag/ZnO (Figure 9c), the high mobility of active oxygen generated from Ag_2O and Ag° corresponds to the high rate of light and heavy VOC oxidation, respectively, in the loose contact. This circumstance is similar to that of Ag/TiO_2. Interestingly, at 400−480 °C, the soot combustion activity in loose and tight contact is identical. This expresses that the oxidizer active in this temperature range has a high ability to transfer from the catalyst to the soot. According to the H_2-TPR, the oxidizer reduced at 400−700 °C is derived from lattice oxygen in the ZnO bulk. This demonstrates the benefit of generating highly active oxygen of Ag/ZnO. However, at a temperature higher than 480 °C, the active oxygen from Ag° is still crucial for the combustion of soot.

Figure 9d illustrates the influence of Ag/CeO_2 on DPM oxidation in the loose contact. The active oxygen derived from Ag_2O and Ag° still shows a high level for light and heavy VOC removal, respectively, compared to the tight contact mode. Interestingly, at high temperatures (~400 °C), the loose contact gives a lower rate of heavy VOC oxidation. This is possibly caused by the insufficient active oxygen formulated on Ag°, as indicated by the low quantity of "area of Ag°" in Table 2. Ag/CeO_2 clearly illustrates the poor soot oxidation performance in loose contact, which results from the low quantity and mobility of active oxygen. The soot combustion profile in loose contact is identical to the uncatalyzed oxidation, implying that Ag/CeO_2 does not assist the transfer of active oxygen from Ag° to soot.

Figure 10 demonstrates the effect of the contact mode and support material on the performance of DPM oxidation. In tight contact, the created active oxidizer can transfer readily from the catalyst surface to DPM, resulting in a high rate of DPM combustion.[84] In contrast, the long distance between the catalyst and DPM hinders the mobility of active oxygen in a loose contact. The potential for depleting VOCs (represented by T_{55}) in loose contact is in the following order: Ag/Al_2O_3

https://doi.org/10.1021/acsomega.4c00218
ACS Omega 2024, 9, 19282−19294

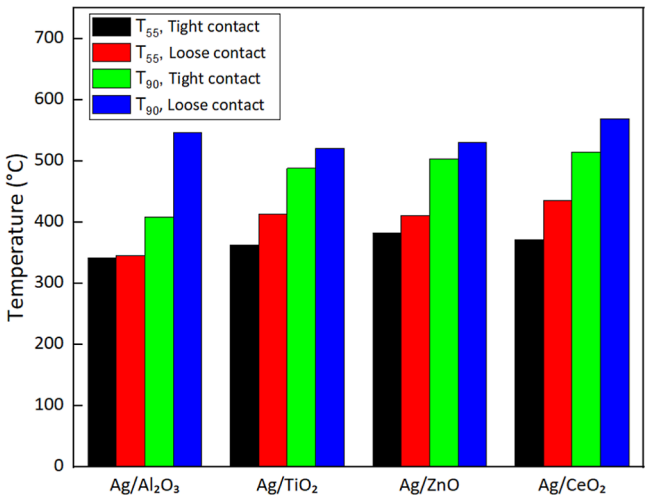

Figure 10. Effect of the contact mode on DPM oxidation performance.

(346 °C) > Ag/ZnO (411 °C) > Ag/TiO_2 (413 °C) > Ag/CeO_2 (435 °C). Interestingly, the loose contact has a negligible effect on the ability to remove VOCs of Ag/Al_2O_3. As mentioned, active oxygen created by and adsorbed on Ag° of Ag/Al_2O_3 originates from gas-phase oxygen. This result suggests that this active oxygen can migrate instantly from the Ag° site to heavy VOCs, even over a long distance. Possibly, adsorbed oxygen is easily induced by the hydrogen atoms of VOCs. In Ag/TiO_2, Ag/ZnO, and Ag/CeO_2, the capability to remove heavy VOCs reduces obviously in the loose contact mode. These catalysts generate active oxygen on the Ag^+ site in the form of Ag_2O, which is reactive with light and heavy VOCs. The result states that the atomic oxygen of Ag_2O has a relatively high bonding strength with Ag^+. To break this bond, Ag_2O needs to be close to heavy VOCs.

T_{90} of loose contact is in the order of Ag/TiO_2 (521 °C), Ag/ZnO (530 °C), Ag/Al_2O_3 (547 °C), and Ag/CeO_2 (569 °C). There is only solid carbon left in the DPM at temperatures after T_{55}. The loose contact significantly impacts the oxidation performance of Ag/Al_2O_3, even though Ag/Al_2O_3 performs excellently in tight contact. It reveals that the active oxygen on the Ag° site of Ag/Al_2O_3 has low mobility in the presence of only carbon atoms. This circumstance contrasts with the case of heavy VOCs, in which hydrogen atoms are present in the DPM. In Ag/TiO_2, Ag/ZnO, and Ag/CeO_2, the loose contact has a relatively low influence on solid-carbon combustion capability, compared with Ag/Al_2O_3. It expresses that the active oxygen formulated from these catalysts has more ability to migrate to solid carbon than that created by Ag/Al_2O_3.

4. CONCLUSIONS

This work studies the positive effect of Ag supported on several supporting materials on DPM oxidation. Ag/Al_2O_3, Ag/TiO_2, Ag/ZnO, and Ag/CeO_2 are synthesized and characterized using H_2-TPR, XRD, HRTEM, XPS, and TGA techniques. Without a catalyst, VOCs are slowly burned at 200−400 °C, and carbonaceous solids are gradually oxidized between 400 and 650 °C. With catalysts, Ag_2O and Ag° are formed in all catalysts, with different contents depending on the support used. Ag_2O plays a crucial role in creating active oxygen that is used for the combustion of light VOCs. This active oxygen shows high performance in both tight and loose contacts due to its high mobility. The catalysts with a high fraction of Ag_2O (e.g., Ag/ZnO and Ag/CeO_2) give a high ability to burn out light VOCs, while Ag/Al_2O_3 with a low extent of Ag_2O shows poor performance for the removal of light VOCs. For the combustion of heavy VOCs and soot, Ag° is of critical importance. The active oxygen formulated on Ag° sites can readily transfer to the hydrogen atom of heavy VOCs even under the loose contact condition; however, it has a low ability to migrate to the carbon atom of soot. Ag/Al_2O_3 with a high portion of Ag° presents the powerful capability to oxidize both heavy VOCs and soot in tight contact. However, it shows poor soot oxidation activity in loose contact due to its low ability to transfer active oxygen. Ag/ZnO facilitates the transfer of active oxygen from Ag° to soot sites, resulting in the high performance of soot oxidation in loose contact conditions.

AUTHOR INFORMATION

Corresponding Author

Boonlue Sawatmongkhon − *College of Industrial Technology, King Mongkut's University of Technology North Bangkok, Bangkok 10800, Thailand; Research Centre for Combustion Technology and Alternative Energy (CTAE), Science and Technology Research Institute, King Mongkut's University of Technology North Bangkok, Bangkok 10800, Thailand;* orcid.org/0000-0001-8972-4387; Email: boonlue.s@cit.kmutnb.ac.th

Authors

Punya Promhuad − *College of Industrial Technology, King Mongkut's University of Technology North Bangkok, Bangkok 10800, Thailand*

Kampanart Theinnoi − *College of Industrial Technology, King Mongkut's University of Technology North Bangkok, Bangkok 10800, Thailand; Research Centre for Combustion Technology and Alternative Energy (CTAE), Science and Technology Research Institute, King Mongkut's University of Technology North Bangkok, Bangkok 10800, Thailand;* orcid.org/0000-0003-0575-324X

Thawatchai Wongchang − *Research Centre for Combustion Technology and Alternative Energy (CTAE), Science and Technology Research Institute, King Mongkut's University of Technology North Bangkok, Bangkok 10800, Thailand; Department of Mechanical and Automotive Engineering Technology, Faculty of Engineering and Technology, King Mongkut's University of Technology North Bangkok (Rayong Campus), Rayong 21120, Thailand*

Nuwong Chollacoop − *Renewable Energy and Energy Efficiency Research Team, National Energy Technology Center (ENTEC), Pathumthani 12120, Thailand*

Ekarong Sukjit − *School of Mechanical Engineering, Institute of Engineering, Suranaree University of Technology, Nakhon Ratchasima 30000, Thailand;* orcid.org/0000-0003-4641-2580

Sarayut Tunmee − *Synchrotron Light Research Institute, Nakhon Ratchasima 30000, Thailand*

Athanasios Tsolakis − *School of Engineering, Mechanical and Manufacturing Engineering, University of Birmingham, Birmingham B15 2TT, U.K.*

Complete contact information is available at: https://pubs.acs.org/10.1021/acsomega.4c00218

https://doi.org/10.1021/acsomega.4c00218
ACS Omega 2024, 9, 19282−19294

Notes

The authors declare no competing financial interest.

■ ACKNOWLEDGMENTS

This research was funded by the National Science, Research and Innovation Fund (NSRF) and King Mongkut's University of Technology North Bangkok under contract no. KMUTNB-FF-66-19. P.P. would like to thank King Mongkut's University of Technology North Bangkok and the National Science and Technology Development Agency, Thailand, for supporting his scholarship under contract no. grad 018/2563, and P.P. would also like to express his sincere gratitude to Prof. Dr. Ekachai Juntasaro for his invaluable support and insightful guidance.

■ REFERENCES

(1) Zhang, Y.; Zhong, Y.; Lu, S.; Zhang, Z.; Tan, D. A Comprehensive Review of the Properties, Performance, Combustion, and Emissions of the Diesel Engine Fueled with Different Generations of Biodiesel. *Processes* **2022**, *10* (6), 1178.

(2) Niu, L.; Wei, T.; Li, Q.; Zhang, G.; Xian, G.; Long, Z.; Ren, Z. Ce-Based Catalysts Used in Advanced Oxidation Processes for Organic Wastewater Treatment: A Review. *J. Environ. Sci.* **2020**, *96*, 109−116.

(3) Scirè, S.; Riccobene, P. M.; Crisafulli, C. Ceria Supported Group IB Metal Catalysts for the Combustion of Volatile Organic Compounds and the Preferential Oxidation of CO. *Appl. Catal., B* **2010**, *101* (1−2), 109−117.

(4) Yamazaki, K.; Kayama, T.; Dong, F.; Shinjoh, H. A Mechanistic Study on Soot Oxidation over CeO_2-Ag Catalyst with "rice-Ball" Morphology. *J. Catal.* **2011**, *282* (2), 289−298.

(5) Gee, I. Volatile Organic Compounds. *Indoor Built Environ.* **1996**, *5* (3), 187−188.

(6) Zeng, L.; Cui, L.; Wang, C.; Guo, W.; Gong, C. Ag-Assisted CeO_2 Catalyst for Soot Oxidation. *Front. Mater. Sci.* **2019**, *13* (3), 288−295.

(7) Pang, L. S. K.; Saxby, J. D.; Chatfield, S. P. Thermogravimetric Analysis of Carbon Nanotubes and Nanoparticles. *J. Phys. Chem.* **1993**, *97* (27), 6941−6942.

(8) Italiano, C.; Bizkarra, K.; Barrio, V. L.; Cambra, J. F.; Pino, L.; Vita, A. Renewable Hydrogen Production via Steam Reforming of Simulated Bio-Oil over Ni-Based Catalysts. *Int. J. Hydrogen Energy* **2019**, *44* (29), 14671−14682.

(9) Xiaowei, L.; Jean-Charles, R.; Suyuan, Y. Effect of Temperature on Graphite Oxidation Behavior. *Nucl. Eng. Des.* **2004**, *227* (3), 273−280.

(10) Shang, D.; Zhong, Q. High Performance of NO Oxidation over $Co/Zr_{0.2}Ce_{0.8}O_2$ Catalysts Prepared by One-Pot Method. *IOP Conf. Ser. Earth Environ. Sci.* **2018**, *186* (2), 012003.

(11) Abián, M.; Martín, C.; Nogueras, P.; Sánchez-Valdepeñas, J.; Rodríguez-Fernández, J.; Lapuerta, M.; Alzueta, M. U. Interaction of Diesel Engine Soot with NO_2 and O_2 at Diesel Exhaust Conditions. Effect of Fuel and Engine Operation Mode. *Fuel* **2018**, *212* (June2017), 455−461.

(12) Kim, T. Y.; Lee, S. H. Combustion and Emission Characteristics of Wood Pyrolysis Oil-Butanol Blended Fuels in a Di Diesel Engine. *Int. J. Automot. Technol.* **2015**, *16*, 903−912.

(13) Li, Z.; Zhang, W.; Chen, Z.; Jiang, Q. Mechanism of Accelerating Soot Oxidation by NO_2 from Diesel Engine Exhaust. *Environ. Pollut.* **2020**, *264* (2), 114708.

(14) Kim, M. J.; Han, G.-H.; Lee, S. H.; Jung, H. W.; Choung, J. W.; Kim, C. H.; Lee, K.-Y. CeO_2 Promoted Ag/TiO_2 Catalyst for Soot Oxidation with Improved Active Oxygen Generation and Delivery Abilities. *J. Hazard. Mater.* **2020**, *384* (September 2019), 121341.

(15) Lee, J. H.; Jo, D. Y.; Choung, J. W.; Kim, C. H.; Ham, H. C.; Lee, K.-Y. Roles of Noble Metals (M = Ag, Au, Pd, Pt and Rh) on CeO_2 in Enhancing Activity toward Soot Oxidation: Active Oxygen Species and DFT Calculations. *J. Hazard. Mater.* **2021**, *403*, 124085.

(16) Diehl, F.; Barbier, J.; Duprez, D.; Guibard, I.; Mabilon, G. Catalytic Oxidation of Heavy Hydrocarbons over Pt/Al_2O_3. Oxidation of C10+ Solid Hydrocarbons Representative of Soluble Organic Fraction of Diesel Soots. *Appl. Catal., A* **2015**, *504*, 37−43.

(17) Gänzler, A. M.; Casapu, M.; Maurer, F.; Störmer, H.; Gerthsen, D.; Ferré, G.; Vernoux, P.; Bornmann, B.; Frahm, R.; Murzin, V.; Nachtegaal, M.; Votsmeier, M.; Grunwaldt, J.-D. Tuning the Pt/CeO_2 Interface by in Situ Variation of the Pt Particle Size. *ACS Catal.* **2018**, *8* (6), 4800−4811.

(18) Nossova, L.; Caravaggio, G.; Couillard, M.; Ntais, S. Effect of Preparation Method on the Performance of Silver-Zirconia Catalysts for Soot Oxidation in Diesel Engine Exhaust. *Appl. Catal., B* **2018**, *225*, 538−549.

(19) Serve, A.; Boreave, A.; Cartoixa, B.; Pajot, K.; Vernoux, P. Synergy between Ag Nanoparticles and Yttria-Stabilized Zirconia for Soot Oxidation. *Appl. Catal., B* **2019**, *242*, 140−149.

(20) Promhuad, P.; Sawatmongkhon, B. Soot Oxidation in Diesel Exhaust on Silver Catalyst Supported by Alumina, Titanium and Zirconium. *E3S Web Conf.* **2021**, *302*, 01008.

(21) Sawatmongkhon, B.; Theinnoi, K.; Wongchang, T.; Haoharn, C.; Wongkhorsub, C.; Sukjit, E.; Tsolakis, A. Catalytic Oxidation of Diesel Particulate Matter by Using Silver and Ceria Supported on Alumina as the Oxidation Catalyst. *Appl. Catal., A* **2019**, *574* (November 2018), 33−40.

(22) Álvarez-Docio, C.; Portela, R.; Reinosa, J. J.; Rubio-Marcos, F.; Fernández, J. F. Pt Mechanical Dispersion on Non-Porous Alumina for Soot Oxidation. *Catal. Commun.* **2020**, *140* (March), 105999.

(23) López-Suárez, F.; Bueno-López, A.; Illán-Gómez, M. J. Cu/Al_2O_3 Catalysts for Soot Oxidation: Copper Loading Effect. *Appl. Catal., B* **2008**, *84* (3−4), 651−658.

(24) Grabchenko, M. V.; Mamontov, G. V.; Zaikovskii, V. I.; La Parola, V.; Liotta, L. F.; Vodyankina, O. V. The Role of Metal-Support Interaction in Ag/CeO_2 Catalysts for CO and Soot Oxidation. *Appl. Catal., B* **2020**, *260* (August 2019), 118148.

(25) Wang, X.; Jin, B.; Feng, R.; Liu, W.; Weng, D.; Wu, X.; Liu, S. A robust core-shell silver soot oxidation catalyst driven by Co_3O_4: Effect of tandem oxygen delivery and Co_3O_4-CeO_2 synergy. *Appl. Catal., B* **2019**, *250* (March), 132−142.

(26) Serhan, N.; Tsolakis, A.; Wahbi, A.; Martos, F. J.; Golunski, S. Modifying Catalytically the Soot Morphology and Nanostructure in Diesel Exhaust: Influence of Silver De-NOx Catalyst (Ag/Al_2O_3). *Appl. Catal., B* **2019**, *241* (September 2018), 471−482.

(27) Chen, L.; Li, T.; Zhang, J.; Wang, J.; Chen, P.; Fu, M.; Wu, J.; Ye, D. Chemisorbed Superoxide Species Enhanced the High Catalytic Performance of Ag/Co_3O_4 Nanocubes for Soot Oxidation. *ACS Appl. Mater. Interfaces* **2021**, *13* (18), 21436−21449.

(28) Aneggi, E.; Llorca, J.; de Leitenburg, C.; Dolcetti, G.; Trovarelli, A. Soot Combustion over Silver-Supported Catalysts. *Appl. Catal., B* **2009**, *91* (1−2), 489−498.

(29) Liu, S.; Wu, X.; Weng, D.; Li, M.; Ran, R. Roles of Acid Sites on Pt/H-ZSM5 Catalyst in Catalytic Oxidation of Diesel Soot. *ACS Catal.* **2015**, *5* (2), 909−919.

(30) Li, Y. F.; Aschauer, U.; Chen, J.; Selloni, A. Adsorption and Reactions of O_2 on Anatase TiO_2. *Acc. Chem. Res.* **2014**, *47* (11), 3361−3368.

(31) Camposeco, R.; Castillo, S.; Hinojosa-Reyes, M.; Nava, N.; Zanella, R. Manganese Promoted TiO_2 and ZrO_2 Nanostructures for Soot Combustion with Boosted Efficiency. *Surf. Coat. Technol.* **2020**, *384* (December2019), 125305.

(32) Li, Y.; Zhang, Y.; Qian, K.; Huang, W. Metal-Support Interactions in Metal/Oxide Catalysts and Oxide-Metal Interactions in Oxide/Metal Inverse Catalysts. *ACS Catal.* **2022**, *12* (2), 1268−1287.

(33) Zhang, Y.; Liu, J.-X.; Qian, K.; Jia, A.; Li, D.; Shi, L.; Hu, J.; Zhu, J.; Huang, W. Structure Sensitivity of Au-TiO_2 Strong Metal-Support Interactions. *Angew. Chem.* **2021**, *133* (21), 12181−12188.

(34) Ma, D.; Wang, Z.; Cui, H.; Zeng, J.; He, C.; Lu, Z. First-Principles Study of O_2 Adsorption on Al-Doped ZnO$(1\ 0\ \bar{1}\ 0)$ Surface. *Sens. Actuators, B* **2016**, *224* (1010), 372−380.

https://doi.org/10.1021/acsomega.4c00218
ACS Omega 2024, 9, 19282−19294

(35) Corro, G.; Cebada, S.; Pal, U.; Fierro, J. L. G. Au^0-Au^{3+} Bifunctional Site Mediated Enhanced Catalytic Activity of Au/ZnO Composite in Diesel Particulate Matter Oxidation. *J. Catal.* **2017**, *347*, 148−156.
(36) Liu, X.; Liu, M. H.; Luo, Y. C.; Mou, C. Y.; Lin, S. D.; Cheng, H.; Chen, J. M.; Lee, J. F.; Lin, T. S. Strong Metal-Support Interactions between Gold Nanoparticles and ZnO Nanorods in CO Oxidation. *J. Am. Chem. Soc.* **2012**, *134* (24), 10251−10258.
(37) Li, P.; Chen, X.; Li, Y.; Schwank, J. W. A Review on Oxygen Storage Capacity of CeO_2-Based Materials: Influence Factors, Measurement Techniques, and Applications in Reactions Related to Catalytic Automotive Emissions Control. *Catal. Today* **2019**, *327* (May), 90−115.
(38) Lee, J. H.; Lee, B. J.; Lee, D. W.; Choung, J. W.; Kim, C. H.; Lee, K. Y. Synergistic Effect of Cu on a Ag-Loaded CeO_2 Catalyst for Soot Oxidation with Improved Generation of Active Oxygen Species and Reducibility. *Fuel* **2020**, *275* (April), 117930.
(39) Lee, J. H.; Lee, S. H.; Choung, J. W.; Kim, C. H.; Lee, K.-Y. Ag-Incorporated Macroporous CeO_2 Catalysts for Soot Oxidation: Effects of Ag Amount on the Generation of Active Oxygen Species. *Appl. Catal., B* **2019**, *246* (November 2018), 356−366.
(40) Wang, C.; Yuan, H.; Lu, G.; Wang, H. Oxygen Vacancies and Alkaline Metal Boost CeO_2 Catalyst for Enhanced Soot Combustion Activity: A First-Principles Evidence. *Appl. Catal., B* **2021**, *281* (June2020), 119468.
(41) Wang, H. F.; Li, H. Y.; Gong, X. Q.; Guo, Y. L.; Lu, G. Z.; Hu, P. Oxygen Vacancy Formation in CeO_2 and $Ce_{1-X}Zr_XO_2$ Solid Solutions: Electron Localization, Electrostatic Potential and Structural Relaxation. *Phys. Chem. Chem. Phys.* **2012**, *14* (48), 16521−16535.
(42) Bueno-López, A.; Krishna, K.; Makkee, M.; Moulijn, J. A. Active Oxygen from CeO_2 and Its Role in Catalysed Soot Oxidation. *Catal. Lett.* **2005**, *99* (3−4), 203−205.
(43) Setiabudi, A.; Chen, J.; Mul, G.; Makkee, M.; Moulijn, J. A. CeO_2 Catalysed Soot Oxidation: The Role of Active Oxygen to Accelerate the Oxidation Conversion. *Appl. Catal., B* **2004**, *51* (1), 9−19.
(44) Alcalde-Santiago, V.; Davó-Quiñonero, A.; Lozano-Castelló, D.; Bueno-López, A. On the Soot Combustion Mechanism Using 3DOM Ceria Catalysts. *Appl. Catal., B* **2018**, *234*, 187−197.
(45) Wang, M.; Zhang, Y.; Yu, Y.; Shan, W.; He, H. Surface Oxygen Species Essential for the Catalytic Activity of Ce-M-Sn (M = Mn or Fe) in Soot Oxidation. *Catal. Sci. Technol.* **2021**, *11* (3), 895−903.
(46) Aneggi, E.; de Leitenburg, C.; Dolcetti, G.; Trovarelli, A. Promotional Effect of Rare Earths and Transition Metals in the Combustion of Diesel Soot over CeO_2 and CeO_2-ZrO_2. *Catal. Today* **2006**, *114* (1), 40−47.
(47) Shimizu, K.-I.; Kawachi, H.; Satsuma, A. Study of Active Sites and Mechanism for Soot Oxidation by Silver-Loaded Ceria Catalyst. *Appl. Catal., B* **2010**, *96* (1−2), 169−175.
(48) Meiwes-Broer, K. H. Work Functions of Metal Clusters. *Hyperfine Interact.* **1994**, *89* (1), 263−269.
(49) Zhang, Y.; Chen, M.; Zhang, Z.; Jiang, Z.; Shangguan, W.; Einaga, H. Simultaneously Catalytic Decomposition of Formaldehyde and Ozone over Manganese Cerium Oxides at Room Temperature: Promotional Effect of Relative Humidity on the $MnCeO_x$ Solid Solution. *Catal. Today* **2019**, *327*, 323−333.
(50) Nakajima, H.; Tong-On, A.; Sumano, N.; Sittisard, K.; Rattanasuporn, S.; Euaruksakul, C.; Supruangnet, R.; Jearanaikoon, N.; Photongkam, P.; Chanlek, N.; Songsiriritthigul, P. Photoemission Spectroscopy and Photoemission Electron Microscopy Beamline at the Siam Photon Laboratory. *J. Phys. Conf. Ser.* **2013**, *425* (13), 132020.
(51) Songsiriritthigul, P.; Kjornrattanawanich, B.; Tong-on, A.; Nakajima, H. Design of the First Undulator Beamline for the Siam Photon Laboratory. *Nucl. Instrum. Methods Phys. Res., Sect. A* **2007**, *582* (1), 100−102.
(52) Atribak, I.; Bueno-López, A.; García-García, A. Uncatalysed and Catalysed Soot Combustion under NO_x + O_2: Real Diesel versus Model Soots. *Combust. Flame* **2010**, *157* (11), 2086−2094.
(53) Li, Z.; Liu, P.; Zhang, C. Regulation of Active Oxygen Species in Cu-MnO_x through MOF Templates for Soot Removal. *Energy Fuels* **2021**, *35* (23), 19655−19664.
(54) Liu, H.; Bai, J.; Wang, S.; Li, C.; Guo, L.; Liang, H.; Xu, T.; Sun, W.; Li, H. The Preparation of Silver Nanoparticles/Carbon Nanofibers as Catalyst in the Styrene Epoxidation. *Colloids Surf., A* **2014**, *448* (1), 154−159.
(55) Charisteidis, I. D.; Triantafyllidis, K. S. Propylene Epoxidation by Molecular Oxygen Using Supported Silver Catalysts: Effect of Support Type, Preparation Method and Promotion with Alkali Chloride and/or Steam. *Catal. Today* **2020**, *355* (June), 654−664.
(56) Zhang, M.; Jin, B.; Liu, Y.; Liu, W.; Weng, D.; Wu, X.; Liu, S. Ozone Activated Ag/CeO_2 Catalysts for Soot Combustion: The Surface and Structural Influences. *Chem. Eng. J.* **2019**, *375* (June), 121961.
(57) Lee, C.; Park, J.-I.; Shul, Y.-G.; Einaga, H.; Teraoka, Y. Ag Supported on Electrospun Macro-Structure CeO_2 Fibrous Mats for Diesel Soot Oxidation. *Appl. Catal., B* **2015**, *174*−*175*, 185−192.
(58) Yu, L.; Peng, R.; Chen, L.; Fu, M.; Wu, J.; Ye, D. Ag Supported on CeO_2 with Different Morphologies for the Catalytic Oxidation of HCHO. *Chem. Eng. J.* **2018**, *334*, 2480−2487.
(59) Corro, G.; Vidal, E.; Cebada, S.; Pal, U.; Bañuelos, F.; Vargas, D.; Guilleminot, E. Electronic State of Silver in Ag/SiO_2 and Ag/ZnO Catalysts and Its Effect on Diesel Particulate Matter Oxidation: An XPS Study. *Appl. Catal., B* **2017**, *216*, 1−10.
(60) He, J.; Du, Y.-E.; Bai, Y.; An, J.; Cai, X.; Chen, Y.; Wang, P.; Yang, X.; Feng, Q. Facile Formation of Anatase/Rutile TiO_2 Nanocomposites with Enhanced Photocatalytic Activity. *Molecules* **2019**, *24* (16), 2996.
(61) Mohammed, A. A.; Khodair, Z. T.; Khadom, A. A. Preparation and Investigation of the Structural Properties of α-Al_2O_3 Nanoparticles Using the Sol-Gel Method. *Chem. Data Collect.* **2020**, *29*, 100531.
(62) Liu, J. J. Advanced Electron Microscopy of Metal-Support Interactions in Supported Metal Catalysts. *ChemCatChem* **2011**, *3* (6), 934−948.
(63) Wu, G.; Liu, Y.; Wang, J. Oxidative-Atmosphere-Induced Strong Metal-Support Interaction and Its Catalytic Application. *Acc. Chem. Res.* **2023**, *56* (8), 911−923.
(64) Tang, H.; Su, Y.; Zhang, B.; Lee, A. F.; Isaacs, M. A.; Wilson, K.; Li, L.; Ren, Y.; Huang, J.; Haruta, M.; Qiao, B.; Liu, X.; Jin, C.; Su, D.; Wang, J.; Zhang, T. Classical Strong Metal-Support Interactions between Gold Nanoparticles and Titanium Dioxide. *Sci. Adv.* **2017**, *3* (10), 1−9.
(65) Tang, H.; Wei, J.; Liu, F.; Qiao, B.; Pan, X.; Li, L.; Liu, J.; Wang, J.; Zhang, T. Strong Metal-Support Interactions between Gold Nanoparticles and Nonoxides. *J. Am. Chem. Soc.* **2016**, *138* (1), 56−59.
(66) Ruan, H.; Nishibori, M.; Uchiyama, T.; Ninomiya, K.; Kamitani, K.; Kato, K.; Konishi, Y.; Haensch, A.; Barsan, N.; Weimar, U.; Shimanoe, K. Soot Oxidation Performance with a HZSM-5 Supported Ag Nanoparticles Catalyst and the Characterization of Ag Species. *RSC Adv.* **2017**, *7* (69), 43789−43797.
(67) Ousji, R.; Ksibi, Z.; Ghorbel, A.; Fontaine, C. Ag-Based Catalysts in Different Supports: Activity for Formaldehyde Oxidation. *Adv. Mater. Phys. Chem.* **2022**, *12* (08), 163−176.
(68) Wang, W.; Liu, Y.; Wang, L.; Zhan, W.; Guo, Y.; Guo, Y. Soot Combustion over Ag Catalysts Supported on Shape-Controlled CeO_2. *Catal. Today* **2021**, *376*, 9−18.
(69) Liu, S.; Wu, X.; Tang, J.; Cui, P.; Jiang, X.; Chang, C.; Liu, W.; Gao, Y.; Li, M.; Weng, D. An Exploration of Soot Oxidation over CeO_2-ZrO_2 Nanocubes: Do More Surface Oxygen Vacancies Benefit the Reaction? *Catal. Today* **2017**, *281*, 454−459.
(70) Skaf, M.; Aouad, S.; Hany, S.; Cousin, R.; Abi-Aad, E.; Aboukaïs, A. Physicochemical Characterization and Catalytic Performance of 10% Ag/CeO_2 Catalysts Prepared by Impregnation and Deposition-Precipitation. *J. Catal.* **2014**, *320* (1), 137−146.

https://doi.org/10.1021/acsomega.4c00218
ACS Omega 2024, 9, 19282−19294

(71) Jabłońska, M.; Nocuń, M.; Bidzińska, E. Silver-Alumina Catalysts for Low-Temperature Methanol Incineration. *Catal. Lett.* **2016**, *146* (5), 937−944.
(72) Boccuzzi, F.; Chiorino, A.; Manzoli, M.; Andreeva, D.; Tabakova, T.; Ilieva, L.; Iadakiev, V. Gold, Silver and Copper Catalysts Supported on TiO_2 for Pure Hydrogen Production. *Catal. Today* **2002**, *75* (1−4), 169−175.
(73) Corro, G.; Cebada, S.; Pal, U.; Fierro, J. L. G.; Alvarado, J. Hydrogen-Reduced Cu/ZnO Composite as Efficient Reusable Catalyst for Diesel Particulate Matter Oxidation. *Appl. Catal., B* **2015**, *165*, 555−565.
(74) Zhao, L.; Zhang, Y.; Bi, S.; Liu, Q. Metal-Organic Framework-Derived CeO_2-ZnO Catalysts for C_3H_6-SCR of NO: An: In Situ DRIFTS Study. *RSC Adv.* **2019**, *9* (33), 19236−19242.
(75) Queiroz, C. M. S.; Machado, A. P.; Paiva, A. R. N.; Antoniassi, R. M.; Vaz, J. M.; Spinacé, E. V. Active Pt/CeO_2 Catalysts Prepared by an Alcohol-Reduction Process for Low-Temperature CO-PROX Reaction. *Mater. Renew. Sustain. Energy* **2019**, *8* (3), 17.
(76) Wei, Y.; Liu, J.; Zhao, Z.; Xu, C.; Duan, A.; Jiang, G. Structural and Synergistic Effects of Three-Dimensionally Ordered Macroporous $Ce_{0.8}Zr_{0.2}O_2$-Supported Pt Nanoparticles on the Catalytic Performance for Soot Combustion. *Appl. Catal., A* **2013**, *453*, 250−261.
(77) Yao, H. C.; Yao, Y. F. Y. Ceria in Automotive Exhaust Catalysts. I. Oxygen Storage. *J. Catal.* **1984**, *86* (2), 254−265.
(78) Grabchenko, M. V.; Mikheeva, N. N.; Mamontov, G. V.; Salaev, M. A.; Liotta, L. F.; Vodyankina, O. V. Ag/CeO_2 Composites for Catalytic Abatement of CO, Soot and VOCs. *Catalysts* **2018**, *8* (7), 285.
(79) Iamcheerangkoon, T.; Chollacoop, N.; Sawatmongkhon, B.; Wongchang, T.; Sittichompoo, S.; Chuepeng, S.; Theinnoi, K. Promotion of the NO-to-NO_2 Conversion of a Biofueled Diesel Engine with Nonthermal Plasma-Assisted Low-Temperature Soot Incineration of a Diesel Particulate Filter. *Energies* **2022**, *15* (24), 9330.
(80) Charisiou, N. D.; Tzounis, L.; Sebastian, V.; Hinder, S. J.; Baker, M. A.; Polychronopoulou, K.; Goula, M. A. Investigating the Correlation between Deactivation and the Carbon Deposited on the Surface of Ni/Al_2O_3 and Ni/La_2O_3-Al_2O_3 Catalysts during the Biogas Reforming Reaction. *Appl. Surf. Sci.* **2019**, *474* (November 2017), 42−56.
(81) Santamaria, L.; Lopez, G.; Arregi, A.; Amutio, M.; Artetxe, M.; Bilbao, J.; Olazar, M. Stability of Different Ni Supported Catalysts in the In-Line Steam Reforming of Biomass Fast Pyrolysis Volatiles. *Appl. Catal., B* **2019**, *242* (September 2018), 109−120.
(82) Kundakovic, L.; Flytzani-Stephanopoulos, M. Deep Oxidation of Methane over Zirconia Supported Ag Catalysts. *Appl. Catal., A* **1999**, *183* (1), 35−51.
(83) Ramdas, R.; Nowicka, E.; Jenkins, R.; Sellick, D.; Davies, C.; Golunski, S. Using Real Particulate Matter to Evaluate Combustion Catalysts for Direct Regeneration of Diesel Soot Filters. *Appl. Catal., B* **2015**, *176−177* (2), 436−443.
(84) Neha; Prasad, R.; Singh, S. V. A Review on Catalytic Oxidation of Soot Emitted from Diesel Fuelled Engines. *J. Environ. Chem. Eng.* **2020**, *8* (4), 103945.

https://doi.org/10.1021/acsomega.4c00218
ACS Omega 2024, 9, 19282−19294